Texture Features Based Detection of Parkinson's Disease on DaTSCAN Images*

Francisco Jesús Martínez-Murcia[1], Juan Manuel Górriz[1], Javier Ramírez[1], I. Alvarez Illán[1], and C.G. Puntonet[2]

[1] Department of Signal Theory, Networking and Communications, Universidad of Granada, Spain
[2] Department of Computer Architecture and Technology, Universidad de Granada, Spain

Abstract. In this work, a novel approach to Computer Aided Diagnosis (CAD) system for the Parkinson's Disease (PD) is proposed. This tool is intended for physicians, and is based on fully automated methods that lead to the classification of Ioflupane/FP-CIT-I-123 (DaTSCAN) SPECT images. DaTSCAN images from the Parkinson Progression Markers Initiative (PPMI) are used to have in vivo information of the dopamine transporter density. These images are normalized, reduced (using a mask), and then a GLC matrix is computed over the whole image, extracting several Haralick texture features which will be used as a feature vector in the classification task. Using the leave-one-out cross-validation technique over the whole PPMI database, the system achieves results up to a 95.9% of accuracy, and 97.3% of sensitivity, with positive likelihood ratios over 19, demonstrating our system's ability on the detection of the Parkinson's Disease by providing robust and accurate results for clinical practical use, as well as being fast and automatic.

Keywords: Parkinson's Disease, DaTSCAN images, Computer Aided Diagnosis, Haralick Texture Features, Support Vector Machines, Supervised Learning.

1 Introduction

Parkinsonian Syndrome (PS), also known as Parkinsonism, is a neurological syndrome characterized by tremor, hypokinesia, rigidity and postural instability [3]. It is considered as the second most common neurodegenerative disease, with a prevalence of 1-3% in the population over 65 years of age [11]. A wide range of etiologies may lead to the PS, while the most common cause is the neurodegenerative condition called Parkinson's Disease (PD). This disease originates due to

* Data used in the preparation of this article were obtained from the Parkinson's Progression Markers Initiative (PPMI) database (`www.ppmi-info.org/data`). As such, the investigators within PPMI contributed to the design and implementation of PPMI and/or provided data but did not participate in the analysis or writing of this report. PPMI investigators include (complete listing at PPMI site).

J.M. Ferrández Vicente et al. (Eds.): IWINAC 2013, Part II, LNCS 7931, pp. 266–277, 2013.

the progressive loss of dopaminergic neurons of the nigrostriatal pathway, which connects the substantia nigra to the striatum. As a result, the dopamine content of the striatum decreases, and consequently, dopamine transporters (DAT) are lost. Other possible causes include some toxins, a few metabolic diseases, and a handful of non-PD neurological conditions [2].

As the PD is related to a loss of dopamine transporters in the nigrostriatal pathway, the study of its status by means of brain imaging techniques has been suggested to increase the diagnostic accuracy in the case of parkinsonian syndromes [3]. Ioflupane/FP-CIT-I-123 (better known as DaTSCAN) is a tracer that binds to the dopamine transporters in the striatum, allowing the obtention of Single Photon Emission Computed Tomography (SPECT) images that show a reduced uptake of the tracer in the striatum in patients with PS [1].

A wide range of supervised learning techniques have been combined to generate Computer Aided Diagnosis (CAD) systems that allow to detect neurodegenerative diseases, such as Alzheimer's Disease [9] or Parkinson [16]. Techniques range from the use of selection of Regions of Interest (ROIs) [5], or Single Value Decomposition strategies (SVD) [14] to more complex approaches such as Empirical Mode Decomposition (EMD) combined with Principal Component Analysis (PCA) combined method in [13].

In this work we use the Haralick Texture analysis, proposed in [4], that provides several texture features, which we will use to characterize some patterns of the Parkinson's Disease. To do so, we calculate a 3D Gray Level Co-occurrence (GLC) matrix [12], required for the computation of these features. Finally we make use of a Support Vector Machine (SVM) [18] binary classifier to test the ability of these features in the PD pattern detection.

2 Methodology

2.1 Test Data and Preprocessing

Data used in the preparation of this article were obtained from the Parkinson's Progression Markers Initiative (**PPMI**) database (`www.ppmi-info.org/data`). For up-to-date information on the study, visit `www.ppmi-info.org`.

The images in this database were imaged 4 ± 0.5 hours after the injection of between 111 and 185 MBq of DaTSCAN. Subjects were also pretreated with saturated iodine solution (10 drops in water) or perchlorate (1000 mg) prior to the injection. All subjects had a supplied ^{57}Co line marker affixed along the canthomeatal line, which will facilitate subsequent image processing and allow the core lab to accurately distinguish left and right in the face of multiple image file transfers. These markers are only evident in the ^{57}Co window and hence do not contaminate the ^{123}I-DaTSCAN brain data [8,6].

Raw projection data are acquired into a 128×128 matrix stepping each 3 degrees for a total of 120 projection into two 20% symmetric photopeak windows centered on 159 KeV and 122 KeV with a total scan duration of approximately 30 - 45 minutes. Other scan parameters (collimation, acquisition mode, etc) are

selected for each site. The images of both the subject's data and the cobalt striatal phantom are reconstructed and attenuation corrected, implementing either filtered back-projection or an iterative reconstruction algorithm using standardized approaches [6]. After the processing, images used are spatially and intensity normalized, and of a $91 \times 109 \times 91$ size.

All images in the databases have been spatially normalized (using the **SPM8** software and a custom DaTSCAN template -see Fig. 1, which depicts some cuts of both normal and affected subjects-) and intensity normalized using the **Integral Normalization** algorithm. This method is based on the obtainment of an intrinsic parameter from the image, I_p, and the estimation of the binding activity as:

$$t' = t/I_p \tag{1}$$

where t denotes the spatially normalized image, and t' the image normalized spatially and in intensity. In this case, all intensity values on the image are summed as an aproximation of the expression $I_p = \int t$, which results in an integral value of the intensity.

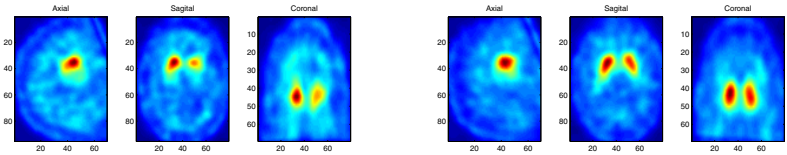

(a) PD subject (PPMI) (b) Normal Control (PPMI)

Fig. 1. Sample image from (a) a PD patient from PPMI database and (b) a healthy subject from PPMI database

2.2 Mask

At this point, all the images are spatially and intensity normalized. These images feature two major changes in their intensity levels: the change between the noisy background and the whole brain, and the increase difference between brain intensity levels and those of the striatum.

We assume that the change between the background and the brain should not be significative enough for the diagnosis of the PD, though its influence on the texture of the image is clear. Given this assumption, it would be desirable to remove all background pixels from the images. To do so, we use a **masking process**.

As the computation of the GLC matrix (which will be explained more extensively in the following section) needs an cuboid image, our purpose is to extract the biggest box which contains only brain pixels. Thus, we establish an intensity threshold, I_{th}, and extract a mask from the mean image of all images in the database using:

$$Mask = I > I_{th} \tag{2}$$

Then, the coordinates of the largest box that fits into that mask is obtained, and this area is selected in all images. We have used intensity thresholds ranging from 0% (all image is selected) to 50% of the highest intensity of the mean image.

2.3 Haralick Texture Features

A co-occurrence matrix is a matrix that is defined over an image to be the distribution of co-occurring values at a given offset. Mathematically, a co-occurrence matrix $\mathbf{C}$ is defined over an $n \times m$ image $\mathbf{I}$, parameterized by an offset (Δx,Δy), as:

$$\mathbf{C}_{\Delta x,\Delta y}(i,j) = \sum_{p=1}^{n}\sum_{q=1}^{m} \begin{cases} 1, & \text{if } \mathbf{I}(p,q) = i \text{ and } \mathbf{I}(p+\Delta x, q+\Delta y) = j \\ 0, & \text{otherwise} \end{cases} \tag{3}$$

Note that the (x,y) parameterization makes the co-occurrence matrix sensitive to rotation. We choose one offset vector, so a rotation of the image not equal to 180 degrees will result in a different co-occurrence distribution for the same (rotated) image. This is rarely desirable in the applications co-occurrence matrices are used in, so the co-occurrence matrix is often formed using a set of offsets sweeping through 180 degrees (i.e. 0, 45, 90, and 135 degrees) at the same distance to achieve a degree of rotational invariance.

The method used here to expand the co-occurrence matrix to a tridimensional space is defined in [12], introducing another variable in Eq. 3. A 3D co-occurrence matrix $\mathbf{C}$ is defined over an $n \times m \times k$ three-dimensional image $\mathbf{I}$, parameterized by an offset (Δx,Δy, Δz), as:

$$\mathbf{C}_{\Delta}(i,j) = \sum_{p=(1,1,1)}^{(n,m,k)} \begin{cases} 1, & \text{if } \mathbf{I}(\mathbf{p}) = i \text{ and } \mathbf{I}(\mathbf{p}+\Delta) = j \\ 0, & \text{otherwise} \end{cases} \tag{4}$$

where i and j are different gray levels, $\mathbf{p} = (x, y, z)$ is the spatial position and Δ is the offset vector.

$$\mathbf{p} = (p, q, r), \text{ and } \Delta = (\Delta x, \Delta y, \Delta z) \tag{5}$$

Twelve Haralick texture features [4] are then extracted from the GLC matrix computed in Eq. 4, in this order: Energy, Entropy, Correlation, Contrast, Variance, Sum Average, Inertia, Cluster shade, Cluster prominence, Homogeneity, Maximum probability and Inverse variance. As 13 spatial directions and 10 distances are considered, a total number of 130 co-ocurrence matrices are computed, and therefore, 130 values for each of the Haralick texture features have been computed. These values have been used as an input vector to the following classifier.

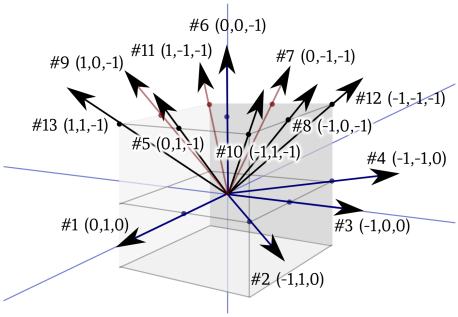

Fig. 2. Spatial representation of the thirteen direction vectors used to compute the thirteen different GLC matrices

2.4 Classifier

The classification step is performed as follows. A predictive model is derived from a set of training data from two different classes -in our case, patients without dopaminergic deficit (NOR) and Parkinson's Disease (PD)-, and the test image is then classified. To build our predictive model, we make use of the Support Vector Machines paradigm. Support Vector Machine (SVM) [17] is a recent class of statistical classification and regression techniques playing an increasing role in applications to detection problems in various engineering problems, notably in statistical signal processing, pattern recognition, image analysis [9], and communication systems. SVM with linear discriminant functions define decision hypersurfaces or hyperplanes in a multidimensional feature space, that is:

$$g(\mathbf{x}) = \mathbf{w}^T\mathbf{x} + \omega_0 = 0, \tag{6}$$

where $\mathbf{w}$ is known as the weight vector and ω_0 as the threshold. The weight vector $\mathbf{w}$ is orthogonal to the decision hyperplane and the optimization task consists of finding the unknown parameters $\omega_i, i = 1, ..., n$ defining the decision hyperplane.

Let $\mathbf{x_i}, i = 1, 2, ..., n$ be the feature vectors of the training set, X. These belong to either ω_1 or ω_2, the two classes. If the classes were linearly separable, the objective would be to design a hyperplane that classifies correctly all the training vectors. Among the different design criteria, the maximal margin hyperplane is usually selected since it leaves the maximum margin of separation between the two classes. Since the distance from a point $\mathbf{x}$ to the hyperplane is given by $z = |g(\mathbf{x})|/\|\mathbf{w}\|$, scaling w and $\mathbf{w_0}$ so that the value of $g(\mathbf{x})$ is $+1$ for the nearest point in ω_1 and -1 for the nearest points in ω_2, the optimization problem is reduced to minimizing a cost function $J(\boldsymbol{\omega}) = 1/2||\boldsymbol{\omega}||^2$ subject to:

$$f_{svm}(\mathbf{x}) = \sum_{i=1}^{N_S} \alpha_i \omega_i \Phi(\mathbf{s}_i) \cdot \Phi(\mathbf{x}) + \omega_0 \tag{7}$$

where α_i are the solution of a quadratic optimization problem that is usually determined by quadratic programming or the well-known sequential minimal optimization algorithm, and $\Phi(\mathbf{s})$ or $\Phi(\mathbf{x})$ denote the transformation of the feature vectors into the effective feature space. This basic SVM classifier produces a linear separation hyperplane.

SVM classifiers with linear kernels are based on a solid theoretical background thus leading to reproducible performance and finally, showing a good robustness to noisy or mislabeled data. Therefore, they are usually applied to evaluate the separability of different features, providing low generalization error even with small learning sample datasets.

3 Results and Discussion

To perform an evaluation of our proposed CAD system, we have independently evaluated the effect of using each of the 12 Haralick Texture Features. Thus, regarding their ability to correctly interpret the texture of the normalized DaTSCAN image. All directions are considered but the influence of the distance d at whith the GLC matrix is calculated has been also considered, using all the feature values extracted in a range of $1 < d$ distance from the central voxel.

In each of these experiments, the images are previously reduced using masks, with an specific intensity threshold I_{th} starting at 0% (whole image) up to 50% of the highest intensity value, as commented in Section 2.2.

3.1 Evaluation

The proposed methodology has been tested on the PPMI databse (see Sec. 2.1). We have used a cross-validation method called leave-one-out to extract some evaluation parameters which will allow us to compare and evaluate the performance of these proposed systems. Parameters like accuracy, sensitivity, specificity, Positive Likelihood (PL) and Negative Likelihood (NL) ratios have been estimated using this method.

Leave-one-out method provides us with a mean of using almost all images for the training of the classifier and still get an unbiased error estimate [7]. However this estimate might be affected by the database topology and the classifier used. Anyway, this is one of the most used methods for system validation, and so will be used in this work.

The accuracy, sensitivity and specificity parameters are calculated as:

$$\text{Acc} = \frac{TP + TN}{TP + TN + FP + FN}, \text{Sens} = \frac{TP}{TP + FN}, \text{ Spec} = \frac{TN}{TN + FP} \tag{8}$$

where *TP*, *TN*, *FP* and *FN* are the number of true positives, true negatives, false positives and false negatives, respectively. Accuracy measures the proportion of correctly classified samples. Sensitivity and specificity are used to measure the proportion of actual positives or negatives which are identified correctly (e.g. the percentage of PS patients, or normal controls who are identified as such).

Although sensitivity and specificity are very important to reveal the ability of a system on detecting PD/NOR patterns, they are prevalence-dependent. This means that in an positive prevalent database (those where there is a higher number of positives), sensitivity will be higher, and similarly occurs with specificity. So even if they are a good estimate of the goodness of the classifier, other parameters such as Positive and Negative Likelihood ratios (PL and NL), which are prevalence independent, are computed.

$$PL = \text{Sensitivity}/(1 - \text{Specificity}) \tag{9}$$

$$NL = (1 - \text{Sensitivity})/\text{Specificity} \tag{10}$$

These parameters are also widely used in clinical medicine, where values of PL greater than 5 or NL values less than 0.2 can be applied to the pre-test probability of a patient having the disease tested to estimate a post-test probability of the disease state existing [10]. A positive result for a test with PL of 8 adds approximately 40% to the pre-test probability that a patient has a specific diagnosis. These parameters are computed with Eq. 9 and 10.

3.2 Results and Discussion

In this work, we have tested the performance of a CAD system which makes use of the Haralick Texture Features to extract relevant textural information from images, and then using these features to classify each image. We have used a mask to reduce dimensionality and improve the GLC matrix computation, and the whole system has been evaluated using the widely available PPMI database, to better facilitate the reproducibility of results.

As commented in Section 2.2, a mask has been added to the normalized images, to extract smaller box-shaped images that allows us to both perform the following tests more efficiently and optimize the calculation of the GLC matrix by removing all non-brain pixels from the source image. Therefore, this masking step might seem profitable.

However, it shows one major drawback: its dependence on the manual operation of setting the mask threshold. Although large number of border detection algorithms exist, and most of them could be applied here to select the brain area, and thus, the intensity threshold, in this work we have established some manual thresholds -see Sec. 2.2- for better evaluating the performance of our system.

To better illustrate the influence of using masks, Table 1 shows the accuracy results obtained by our system using either no mask (mask = 0%) or different levels for the intensity threshold I_{th}.

Most of the best values are obtained using the Homogeneity as an input vector, except for when $I_{th} > 0.35 * I_{max}$. This can be easily explained due to the image characteristics. As we commented before, one of the reasons of using masks was to select the biggest image box that contains only brain pixels. This is achieved in these integral-normalized images when the intensity threshold values

Table 1. Accuracy results for each of the 12 Haralick texture features (see Sec. 2.3), using different intensity thresholds (in %)

Feature	0	5%	15%	25%	35%	45%
Energy	0.822	0.822	0.784	0.862	0.929	0.952
Entropy	0.807	0.807	0.792	0.881	0.933	0.914
Correlation	0.851	0.851	0.870	0.929	0.933	0.955
Contrast	0.818	0.818	0.833	0.937	0.948	0.937
Variance	0.762	0.762	0.784	0.825	0.888	0.914
Sum Average	0.810	0.810	0.844	0.900	0.937	0.933
Inertia	0.773	0.773	0.810	0.833	0.937	0.941
ClusterShade	0.818	0.818	0.833	0.937	0.948	0.937
ClusterTendency	0.926	0.926	0.911	0.941	0.933	0.918
Homogeneity	0.926	0.926	0.929	0.944	0.952	0.907
MaxProbability	0.766	0.766	0.747	0.770	0.818	0.814
InverseVariance	0.743	0.743	0.796	0.870	0.874	0.914

are around this percentage of the maximum intensity of the image. Therefore, more automatic methods to detect this threshold in all types of images should be desirable. In Figure 3, the resulting area of using an $I_{th} = 0.30 I_{max}$ is depicted, applied to the same subject on Fig. 1b. It is interesting to note that our goal of selecting only internal brain voxels has been achieved with this threshold.

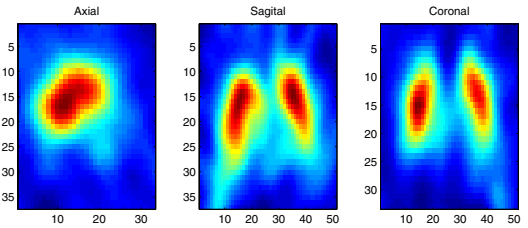

Fig. 3. Resulting image box when using a mask with a $I_{th} = 0.30 I_{max}$

As commented before, all features improve their accuracy results as the intensity threshold increases, but there are some of them that perform particularly well in this task, e.g. Homogeneity, Cluster Shade or Energy. Five of these best features are depicted on Fig. 4. It is noticeable that, while some features increase their performance significantly once I_{th} exceeds some values (which we can consider as an indication that only brain voxels have been selected), there are others that offer good values almost independently of the chosen value for I_{th}.

We have already focused on the performance of the system depending on the mask applied and the feature used for classifying. Nevertheless, there is one more

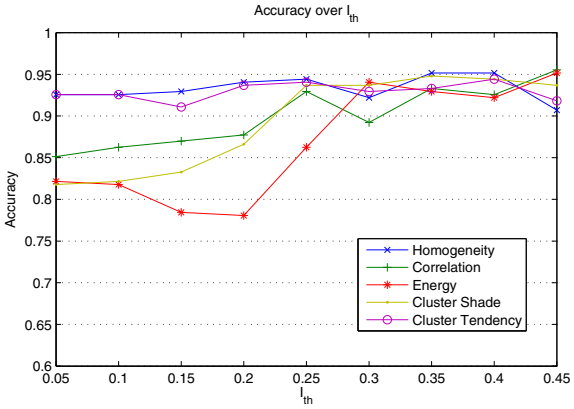

Fig. 4. Accuracy obtained by our proposed system using each of the texture features listed in the legend, using different values for I_{th}

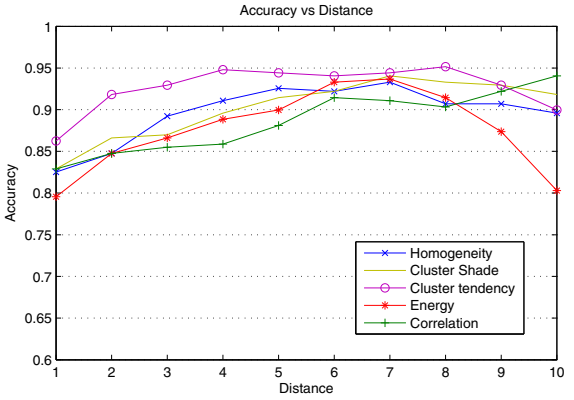

Fig. 5. Accuracy obtained by our proposed system using only the features extracted from the 13 GLC matrices (one in each direction) computed at a distance d of the central voxel

parameter on the system that can affect the results: the distance d at which the GLC matrix is calculated. To perform a deeper analysis of this parameter, we have evaluated the behavior of the system using only the 13 values of each Haralick texture feature extracted from the 13 GLC matrices (one in each direction) computed at a distance d of the central voxel, with $1 < d < 10$. When using each of the five aforementioned texture features, the performance results on our system are displayed on Fig. 5. Notice that, once a maximum is achieved generally at $d = 7, 8$, the accuracy decreases, what might point out the softness degree of the texture pattern of these images.

Table 2. Comparison of our proposed system (using different texture features) and some other methods in the bibliography: VAF system using the intensity-normalized images, a combination of intensity normalization strategies and classifiers (VAF-IN) [5], a SVD-based approach [14] and EMD using the third independent mode function (IMF3) [13].

System	Acc	Sens	Spec	PL	NL
Homogeneity	0.959	0.973	0.949	19.22	0.028
Cluster Shade	0.955	0.964	0.949	19.01	0.038
Cluster Tendency	0.955	0.973	0.943	17.10	0.029
Correlation	0.941	0.946	0.937	14.92	0.058
Energy	0.937	0.964	0.918	11.73	0.039
VAF	0.840	0.807	0.862	5.88	0.224
VAF-IN	0,913	0.890	0.932	13.08	0.118
SVD	0.940	0.962	0.918	11.73	0.041
EMD-IMF3	0.950	0.951	0.948	18.28	0.051

In Table 2 we compare this method with others from the bibliography and the Voxels-as-Features approach, commonly used as an estimation of the performance of visual analysis performed by experts [15]. Some of the methods evaluated include a combination of intensity normalization strategies and classifiers (VAF-IN) [5], a SVD approach that independently decomposes each side of the brain (as PD often show asymmetrical dopamine deficit) [14] and a EMD of the images, then modeled using PCA or ICA to classify the images [13].

Our method based on the Haralick Texture Features and a mask obtains better results in almost every case (specially when using one of the three best features: Homogeneity, Cluster Shade or Cluster Tendency), which also show a high independence of the value used for the intensity threshold of the mask (I_{th}). All methods clearly outperforms the VAF approach, and only the EMD based method obtains similar values to our system. In the latter case, our system shows a clear advantage: its simplicity in terms of computation. While we make use of the directly-computed texture features from the GLC matrix, after a reduction of the image using a mask, the EMD-based method combines gaussian filtering, a Multidimensional Ensemble EMD extraction of some slices, feature reduction using PCA and classification using SVM.

4 Conclussion

The development of new computer-based diagnosis software is a promising area of research. The proposed system aims to provide a fully automated method for physicians to help them in the diagnosis task of Parkinson's Disease (PD), eliminating expensive manual operations, in the sense of requiring an expertise degree of the operator, as well as reducing time costs. Moreover, as the process is automatic, it might not suffer from the pitfalls of investigator-dependent methods.

The presented work makes use of several widely known techniques that, combined, demonstrate their ability in the detection of some PD patterns in DaTSCAN imaging. Particularly, the use of a mask to select subimages that contains only brain voxels has a great impact on the computation of a GLC matrix, facilitating a subsequent texture analysis. Therefore, our system that combines a voxel selection based on mask and the analysis of the textural features of the image demonstrates its ability on the detection of PD patterns in DaTSCAN imaging, providing robust and accurate results up to a 95.9% of accuracy, and 97.3% of sensitivity, with a Positive likelihood ratio over 19, a very good indicator of its robustness on PD detection.

The results hereby presented are very promising, so new approaches to the usage of textural information for the pattern characterization of neurodegenerative disorders can be made.

Acknowledgements. PPMI –a public-private partnership– is funded by The Michael J. Fox Foundation for Parkinson's Research and funding partners, including Abbott, Biogen Idec, F. Hoffman-La Roche Ltd., GE Healthcare, Genentech and Pfizer Inc.

This work was partly supported by the MICINN under the TEC2008-02113 and TEC2012-34306 projects and the Consejería de Innovación, Ciencia y Empresa (Junta de Andalucía, Spain) under the Excellence Projects P07-TIC-02566, P09-TIC-4530 and P11-TIC-7103.

References

1. Bhidayasiri, R.: How useful is (123I) beta-CIT SPECT in the diagnosis of parkinson's disease? Reviews in Neurological Diseases 3(1), 19–22 (2006) PMID: 16596082, http://www.ncbi.nlm.nih.gov/pubmed/16596082
2. Christine, C.W., Aminoff, M.J.: Clinical differentiation of parkinsonian syndromes: Prognostic and therapeutic relevance. The American Journal of Medicine 117(6), 412–419 (2004), http://www.sciencedirect.com/science/article/pii/S0002934304003626
3. Eckert, T., Edwards, C.: The application of network mapping in differential diagnosis of parkinsonian disorders. Clinical Neuroscience Research 6(6), 359–366 (2007), neural Networks in the Imaging of Neuropsychiatric Diseases, http://www.sciencedirect.com/science/article/pii/S1566277207000023
4. Haralick, R., Shanmugam, K., Dinstein, I.: Textural features for image classification. IEEE Transactions on Systems, Man and Cybernetics 3(6), 610–621 (1973)
5. Illán, I., Górriz, J., Ramírez, J., Segovia, F., Jiménez-Hoyuela, J., Ortega Lozano, S.: Automatic assistance to parkinsons disease diagnosis in datscan spect imaging. Medical Physics 39(10), 5971–5980 (2012)
6. The Parkinson Progression Markers Initiative: PPMI. Imaging Technical Operations Manual, 2 edn. (June 2010)
7. Kohavi, R.: A study of cross-validation and bootstrap for accuracy estimation and model selection. In: Proceedings of International Joint Conference on AI, pp. 1137–1145 (1995), http://citeseer.ist.psu.edu/kohavi95study.html

8. Marek, K., Jennings, D., Lasch, S., Siderowf, A., Tanner, C., Simuni, T., Coffey, C., Kieburtz, K., Flagg, E., Chowdhury, S., Poewe, W., Mollenhauer, B., Klinik, P., Sherer, T., Frasier, M., Meunier, C., Rudolph, A., Casaceli, C., Seibyl, J., Mendick, S., Schuff, N., Zhang, Y., Toga, A., Crawford, K., Ansbach, A., De Blasio, P., Piovella, M., Trojanowski, J., Shaw, L., Singleton, A., Hawkins, K., Eberling, J., Brooks, D., Russell, D., Leary, L., Factor, S., Sommerfeld, B., Hogarth, P., Pighetti, E., Williams, K., Standaert, D., Guthrie, S., Hauser, R., Delgado, H., Jankovic, J., Hunter, C., Stern, M., Tran, B., Leverenz, J., Baca, M., Frank, S., Thomas, C., Richard, I., Deeley, C., Rees, L., Sprenger, F., Lang, E., Shill, H., Obradov, S., Fernandez, H., Winters, A., Berg, D., Gauss, K., Galasko, D., Fontaine, D., Mari, Z., Gerstenhaber, M., Brooks, D., Malloy, S., Barone, P., Longo, K., Comery, T., Ravina, B., Grachev, I., Gallagher, K., Collins, M., Widnell, K.L., Ostrowizki, S., Fontoura, P., Ho, T., Luthman, J., van der Brug, M., Reith, A.D., Taylor, P.: The parkinson progression marker initiative (PPMI). Progress in Neurobiology 95(4), 629–635 (2011), http://www.sciencedirect.com/science/article/pii/S0301008211001651
9. Martínez-Murcia, F., Górriz, J., Ramírez, J., Puntonet, C., Salas-González, D.: Computer aided diagnosis tool for Alzheimer's disease based on Mann-Whitney-Wilcoxon U-test. Expert Systems with Applications 39(10), 9676–9685 (2012)
10. McGee, S.: Simplifying likelihood ratios. Journal of General Internal Medicine 17(8), 646–649 (2002)
11. Moghal, S., Rajput, A.H., D'Arcy, C., Rajput, R.: Prevalence of movement disorders in elderly community residents. Neuroepidemiology 13(4), 175–178 (1994) PMID: 8090259, http://www.ncbi.nlm.nih.gov/pubmed/8090259
12. Philips, C., Li, D., Raicu, D., Furst, J.: Directional invariance of co-occurrence matrices within the liver. In: International Conference on Biocomputation, Bioinformatics, and Biomedical Technologies, pp. 29–34 (2008)
13. Rojas, A., Górriz, J., Ramírez, J., Illán, I., Martínez-Murcia, F., Ortiz, A., Río, M.G., Moreno-Caballero, M.: Application of empirical mode decomposition (emd) on datscan spect images to explore parkinson disease. Expert Systems with Applications 40(7), 2756–2766 (2013), http://www.sciencedirect.com/science/article/pii/S0957417412012274
14. Segovia, F., Górriz, J.M., Ramírez, J., Álvarez, I., Jiménez-Hoyuela, J.M., Ortega, S.J.: Improved parkinsonism diagnosis using a partial least squares based approach. Medical Physics 39(7), 4395–4403 (2012)
15. Stoeckel, J., Ayache, N., Malandain, G., Malick Koulibaly, P., Ebmeier, K.P., Darcourt, J.: Automatic classification of SPECT images of alzheimer's disease patients and control subjects. In: Barillot, C., Haynor, D.R., Hellier, P. (eds.) MICCAI 2004. LNCS, vol. 3217, pp. 654–662. Springer, Heidelberg (2004)
16. Towey, D.J., Bain, P.G., Nijran, K.S.: Automatic classification of 123I-FP-CIT (DaTSCAN) SPECT images. Nuclear Medicine Communications 32(8), 699–707 (2011) PMID: 21659911, http://www.ncbi.nlm.nih.gov/pubmed/21659911
17. Vapnik, V.N.: Estimation of Dependences Based on Empirical Data. Springer, New York (1982)
18. Vapnik, V.N.: Statistical Learning Theory. John Wiley and Sons, Inc., New York (1998)